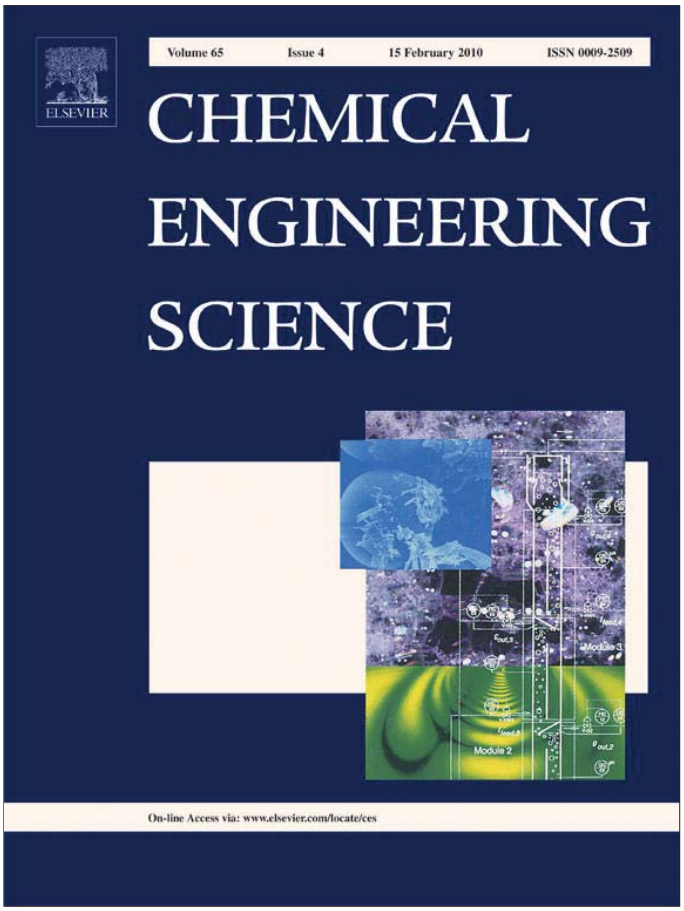

Chemical Engineering Science 65 (2010) 1490–1502

Contents lists available at ScienceDirect

Chemical Engineering Science

journal homepage: www.elsevier.com/locate/ces

Bacterial aerosol neutralization by aerodynamic shocks using an impactor system: Experimental results for *E. coli* and analysis

P.R. Sislian [a], D. Pham [a], X. Zhang [a], M. Li [b], L. Mädler [c], P.D. Christofides [a,d,*]

[a] Department of Chemical and Biomolecular Engineering, University of California, Los Angeles, CA 90095, USA
[b] Department of Chemical and Materials Engineering, California State Polytechnic University, Pomona, CA 91768, USA
[c] Foundation Institute of Materials Science, Department of Production Engineering, University of Bremen, Badgasteiner Str. 3, 28359 Bremen, Germany
[d] Department of Electrical Engineering, University of California, Los Angeles, CA 90095, USA

ARTICLE INFO

Article history:
Received 22 August 2009
Received in revised form
26 October 2009
Accepted 26 October 2009
Available online 4 November 2009

Keywords:
Bacterial aerosol
Aerodynamic shocks
Impactor
Computational modeling
Bacterial break-up
Particle motion
Aerosol sampling
Aerosol collection
Collection efficiency

ABSTRACT

Neutralization of bacterial aerosol releases is critical in countering bioterrorism. As a possible bacterial aerosol neutralization method that avoids the use of chemicals, we investigate the mechanical instabilities of the bacterium cell envelope in air as bacteria are passed through aerodynamic shocks. To carry out this fundamental investigation, an experimental impactor system is developed to collect the bacteria after they pass through a controlled shock, and a detailed computational study is carried out to determine the impactor operating conditions that lead to bacterial break-up. Specifically, the bacteria experience relative deceleration because of sharp velocity changes in the aerodynamic shock created in the experimental impactor system. Computational model results indicate that vegetative *Escherichia coli* cells require a critical acceleration of 3.0×10^8 m/s^2 to break-up. As predicted in computations, experimental findings demonstrate that aerosolized *E. coli* cells that pass through aerodynamic shocks created in the experimental impactor system are an order of magnitude less likely to retain viability than those that pass through the impactor at conditions which do not lead to the generation of an aerodynamic shock, and therefore, do not reach the critical acceleration required for break-up.

1. Introduction

Anthropogenic bacterial aerosols can be used as bioterrorism agents and contribute to the background environmental aerosol. In urban outdoor environments background levels reach 850 cfu/mL (Bovallius et al., 1978; Di Giorgio et al., 1996; Lighthart and Shaffer, 1997; Mancinelli and Shulls, 1978), where cfu refers to colony forming units. Indoor environments contain less bioaerosol. The suspended bacterial particles (both background and anthropogenic) usually range in size from 1 μm (single cells) to 10 μm (multiple cells or cells associated with debris) (Vitko, 2005). In order to effectively mitigate the threat of a biological agent release, effective methods for both sensing and neutralization are necessary.

With respect to sensing, different approaches for biological aerosols have been studied and can be classified into four categories: (1) nucleic acid-based, (2) structure-based, (3) chemistry-based and (4) function-based (Vitko, 2005). Assuming the detection of these agents is possible, current methods are not effective in neutralizing the aerosol cloud at its source and mostly include containment of the aerosol release in order to minimize human exposure. These methods are limited to indoor environments and employ techniques such as high efficiency particulate air (HEPA) filtration, electrostatic precipitation, steam condensation, ultraviolet (UV) inactivation as well as diverting airflows (Vitko, 2005).

The use of aerodynamic shocks holds promise as an alternative way to neutralize bacterial aerosols. The shock can be applied at the point of release both in indoor and outdoor air with the advantage of avoiding chemicals. The aerodynamic shock represents a sharp change in fluid properties (velocity, temperature, pressure). Due to its inertia, a bacterial particle suspended in air will not be able to immediately adjust to a sharp drop in gas velocity and will therefore experience a relative deceleration. Rayleigh–Taylor instabilities in the bacterial membrane arise if the bacterial particle is accelerated (or decelerated) in a perpendicular direction to the bacteria–gas interface (Chandrasekhar, 1961; Joseph et al., 1999). In previous computational work, we have computed the critical accelerations and Weber numbers needed for several bacterial aerosols to break-up (Sislian et al., 2009). Higher surface tension and smaller diameter of the bacterium increase the critical accelerations needed for break-up (Sislian et al., 2009). An impactor system, shown in Fig. 1, has been built and modeled to achieve different bacterial accelerations through a well-defined aerodynamic shock

* Corresponding author at: Department of Chemical and Biomolecular Engineering, University of California, Los Angeles, CA 90095, USA. Tel.: +1 310 794 1015; fax: +1 310 206 4107.
E-mail address: pdc@seas.ucla.edu (P.D. Christofides).

0009-2509/$ - see front matter © 2009 Elsevier Ltd. All rights reserved.
doi:10.1016/j.ces.2009.10.029

(Sislian et al., 2009). After passing through the shock, the bacterial aerosol is collected at low velocity ($<10\,m/s$) to avoid break-up at the point of impaction (Sislian et al., 2009).

A computational model describing the evolution of both gas and particle velocity and temperature was developed for the current impactor system (see Fig. 1) (Sislian et al., 2009). The model calculates accelerations of bacterial particles of up to $10^{10}\,m/s^2$ in the current impactor system. These accelerations are sufficient to break-up gram-negative vegetative *E. coli* cells. However, for example, gram-positive spores of *B. atropheus* which have a higher surface tension and smaller diameter will not reach the critical acceleration required for break-up in the current system (Sislian et al., 2009). Furthermore, to validate the model, the computationally calculated stagnation pressures for different operating conditions were compared with experimental Pitot pressure measurements (Sislian et al., 2009). The calculated and measured data match closely (Sislian et al., 2009).

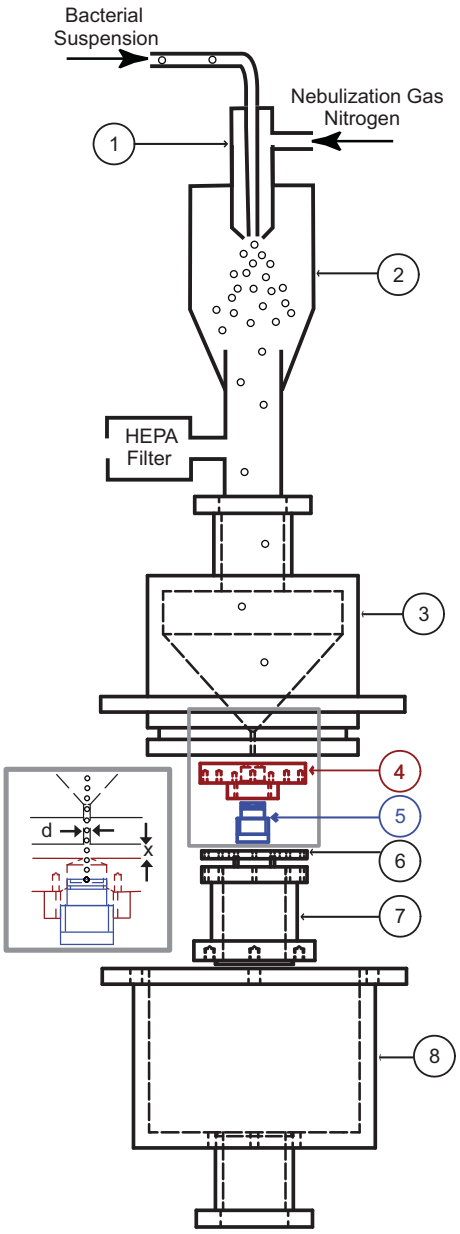

Fig. 1. Schematic of the experimental system. (1) Meinhard nebulizer with a concentric nozzle mixing a liquid bacterial suspension feed and a dispersion gas (N_2), (2) nebulization chamber to collect large droplets, (3) converging nozzle with an exit diameter of $d=0.5$ mm, (4) and (5) a flat surface with a 0.5 mm hole combined with a screw that accommodates the collection substrate make up the deceleration tube, (6) 1.4 mm spacer fixes the spacing x between the impactor and nozzle to 0.6 mm, (7) support holding the deceleration tube and flat surface at fixed distance from the nozzle and (8) exit chamber.

However, the computational model predictions of bacterial neutralization have not been confirmed previously. Some experimental data exist in the literature (Horneck et al., 2001; Lundbeck and Skoldber, 1963; Teshima et al., 1995) on the use of shock waves to neutralize bacteria; however, these studies are limited to bacterial liquid suspensions or powders and do not assess the effects of a shock in the aerosol phase.

The present work focuses on assessing the effect of the aerodynamic shock on *E. coli* cells, which are predicted by our computational model to break-up with our current impactor system. The viability of the *E. coli* is determined after the aerosolized cells pass through the impactor at different operating conditions and are collected. As predicted in computations, experimental findings demonstrate that aerosolized *E. coli* cells that pass through an aerodynamic shock created in the experimental impactor system are an order of magnitude less likely to retain viability than those that pass the impactor at conditions which do not lead to the generation of an aerodynamic shock, and therefore, do not reach the critical accelerations required for break-up.

2. Experimental materials and methods

2.1. Experimental setup

The impactor system discussed in our previous study (Sislian et al., 2009) was used in the experimental setup and is shown in Fig. 1. The bacterial suspension (see Section 2.2) is aerosolized using a capillary nebulizer (TR-30-A1, Meinhard Glass Products) at a gas (N_2) critical flow rate of 0.2 L/min (see Fig. 1; parts 1-2). The impactor (see Fig. 1; parts 3–8) operates at a critical flow rate of 2.3 L/min at shock conditions. As shown in Fig. 1, a high efficiency particulate air (HEPA) filter is installed between the nebulizer (part 2) and the impactor system (part 3) to allow particle-free air to compensate for the higher impactor flow rate, thereby maintaining the upstream impactor pressure at 1 atm.

2.1.1. Nebulization

The phosphate buffered saline (PBS) (BP2438-4, Fisher Scientific) suspension containing the *E. coli* cells (see Section 2.2) is fed via a syringe pump (KDS410, Kd Scientific) at a liquid flow rate $Q=0.05$ mL/min for 20 min. The liquid is fed at a specified bacterial concentration (see Section 2.2) determined by the optical density measurement at 600 nm (OD_{600}). Nitrogen is supplied to the nebulizer at a pressure P_n via a pressurized tank. When the liquid is mixed with the air in the annular region of the nebulizer tip, droplets containing bacterial cells are formed. The bacterial aerosol concentration and droplet size can be adjusted by changing: Q, OD_{600} and P_n. Increasing Q and decreasing P_n increases the average droplet diameter (and volume). Increasing OD_{600} increases the number of cells per volume of liquid nebulized. Collectively, increasing Q and OD_{600} and decreasing P_n increases the number of cells per droplet. With the exception of P_n, Q and OD_{600} also increase the number of cells input into the system in a given time. In all the experiments, the nebulizer was operated at $Q=0.05$ mL/min, $OD_{600}=0.1$, and $P_n=2$ atm. The cell concentration at $OD_{600}=0.1$, as measured using fluorescence cytometry (see Section 2.3), was $2.66\pm0.28\times10^7$ cells/mL. The

expected average nebulized droplet size is 10 μm, which translates to about one cell in every 1000 droplets assuming that no aggregates are formed in the suspension.

In previous liquid suspension shock studies, it has been shown that an increase in cell concentration results in an increase in bacterial viability (Lundbeck and Skoldber, 1963). The controlled bacterial nebulization process produces individual cells suspended in air that can pass isolated through the shock, thereby avoiding the concentration effect seen in liquid suspension studies.

2.1.2. Impactor system

The impactor system consists of a plate designed for the collection of the bacterial aerosol (see Fig. 1; parts 4-5) which is placed perpendicular to the gas flow emerging from a converging nozzle (see Fig. 1; part 3). Isentropic flow theory of an ideal gas predicts a critical downstream (P_1) to upstream (P_0) pressure ratio below which the flow at the exit of the nozzle is sonic (Liepmann and Roshko, 2001; Shapiro, 1953), according to the following equation:

$$\chi_{crit} = (P_1/P_0)_{crit} = [2/(\gamma+1)]^{\gamma/(\gamma-1)}, \quad (1)$$

where γ is the heat capacity ratio ($\gamma = 1.4$; $\chi_{crit} = 0.53$ for N_2). The generated impinging flow on a plate from a converging nozzle operating under sonic conditions results in the creation of a standoff shock whose properties can be changed by varying impactor geometry (distance between nozzle and plate x and diameter of nozzle d) and operating conditions (Alvi et al., 2002; Delamora et al., 1990a, 1990b; Jurcik et al., 1989; Powell, 1988; Sislian et al., 2009). In traditional impactors (Hering et al., 1978, 1979), the aerosol is collected by impaction on a flat surface. Stewart et al. (1995) showed that bacteria collected by impaction are injured; therefore, assessing damage induced by the standoff shock is impossible using current impactor designs. To avoid loss of viability by impaction, the flat surface of the developed impactor system has a central opening (see Fig. 1; part 4) that acts as a virtual surface through which the bacteria enter a stagnant gas deceleration tube (see Fig. 1; parts 4-5). Biswas and Flagan (1988) have designed a similar tube to prevent particle reentrainment. Computational results indicate that the bacteria are collected at low impact velocities (< 10 m/s) in the deceleration tube and consequently will not be injured due to impaction (Sislian et al., 2009). The distance between the opening of the deceleration tube and the nozzle outlet (x) can be adjusted with spacers of different thickness (see Fig. 1; part 6). In the current experimental study, the spacer is 1.4 mm thick. A valve attached to a purge stream downstream of the impactor, controls P_1, whereas the upstream is left at ambient pressure (1 atm).

The deceleration tube is filled with 600 μL of PBS, which keeps the liquid level to about 4 mm away from the entrance of the deceleration tube. The PBS provides a hydration environment for the collected cells and ensures that the collected cells do not lose viability because of drying (this has been experimentally verified). The impactor system with $x/d = 1.2$ was operated for 20 min at three pressure ratios: $\chi = 0.11, 0.50$ and 0.98. As a control to test any low-pressure effects, 600 μL of bacterial suspension (see Section 2.2) at $OD_{600} = 0.01$ was placed in the deceleration tube and the impactor was run with particle-free air for 20 min at the three operating pressures. We experimentally found that cells retain their viability under low pressure conditions when compared with the starting bacterial suspension.

2.2. Bacterial cell culture preparation

E. coli K-12 wild-type strain (MG1655) was used as a standard bacterial aerosol to study the effect of aerodynamic shocks on vegetative bacterial cells in the impactor system. All cell cultures were initiated from a stock *E. coli* suspension (80% glycerol solution) stored at −20 °C. 5 mL of Luria Bertani (LB) broth (Fisher) was inoculated with 3 μL of stock suspension in a test tube. The culture was incubated in a shaker (Excella E24, New Brunswick Scientific) at 37 °C at 200 rpm for approximately 16 h. Subsequently, 2 mL of culture was centrifuged at 4400 rpm for 5 min (Centrifuge 5702, Eppendorf) and washed (3×) with 4 mL PBS. After washing, the optical density of the suspension was measured at a wavelength of 600 nm (OD_{600}) using a visible light spectrophotometer (Genesis 20, Thermo Scientific). The cell suspension was diluted to $OD_{600} = 0.1$ to be used in the experiments described in Section 2.1.1. Another dilution at $OD_{600} = 0.01$ was prepared for suspension flow cytometry measurements, but not nebulized.

A positive and negative control were prepared and carried out before the start of every experiment. The negative control is the cell suspension in PBS diluted to $OD_{600} = 0.01$ as described above. The negative control serves as the starting point for viability measurements. It is the measurement with most viable cells. The positive control was prepared by centrifuging 2 mL of the cell culture at 4400 rpm and washing with 4 mL 70% ethanol. The ethanol-washed cells were incubated for 15 min at room temperature. The suspension was then centrifuged at 4400 rpm and washed (2×) with 4 mL PBS. The positive control was then diluted to $OD_{600} = 0.01$. The effect of aerodynamic shock was then compared to a standard ethanol disinfection method (positive control) used in liquid suspension.

2.3. Bacterial viability analysis

Bacterial viability is determined using LIVE/DEAD® *Bac*Light™ (cat. number L7012; Life Technologies Corporation) (Berney et al., 2007; Laflamme et al., 2004). The assay contains two components: (A) 3.34 mM STYO 9, a green-fluorescent nucleic acid stain, in dimethyl sulfoxide (DMSO) and (B) 20 mM propidium iodide (PI), a red-fluorescent nucleic stain, in DMSO. STYO 9 penetrates both intact and damaged membranes, while PI only penetrates damaged membranes. A stock dye solution is prepared at the start of every experiment by mixing 5 μL of each of components A and B with 10 μL PBS. All controls and experimental samples mentioned in Sections 2.1 and 2.2 were stained with the stock dye solution to a final concentration of 8.35 and 50 μM of STYO 9 and PI, respectively.

The stained samples were analyzed using a fluorescence flow cytometer (FACScan™, BD Biosciences). The cytometer was operated at 12 μL/min for 20 s with a 488 nm excitation laser. Red fluorescence was measured with a high pass filter at 630 nm (FLH-2) and green fluorescence was measured at a bandpass of 520 nm (FLH-1). The forward scatter (FSC) and side scatter (SSC) were also measured for the particles passing the laser. Photomultiplier tubes were used to amplify the optical signal for FLH-1, FLH-2 and SSC at 850, 800 and 375 volts, respectively. A photodiode was used to detect the FSC signal.

2.4. Mass balance analysis

A 0.2 μm black polycarbonate filter (Millipore) was placed in an in-line 25 mm filter holder inserted after the nebulization chamber and before the HEPA filter of the experimental setup shown in Fig. 1. After running the experiment for 20 min, the filter was placed in a Millipore filter holder and 1 mL of a 50 μM STYO 9 stock was passed through the filter staining all cells. After staining, the filter was placed on a microscope slide and 5 μL of mounting oil (cat. number L7012; Life Technologies Corporation)

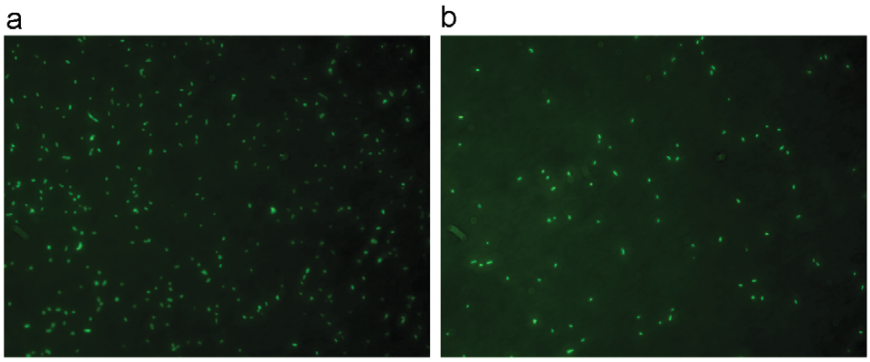

Fig. 2. Fluorescence microscopy images taken at 40× objective lens with an area of $3.8 \times 10^4\ \mu m^2$. The cells are stained with STYO 9 dye which penetrates both live and dead cells. The images are taken for counting purposes and not for determination of cell viability. (a) Image of *E. coli* from cell suspension in PBS at $OD_{600} = 0.01$ on a polycarbonate filter. (b) Image of nebulized *E. coli* collected on an inline filter between the nebulizer and the entrance of the impactor system operated at a flowrate of 2.3 L/min for 20 min.

was added to the surface of the filter, and covered with a glass slip. Images of the filter were taken with a fluorescence microscope at an objective lens magnification of 40× (Zeiss). Each image represents a filter area of $3.8 \times 10^4\ \mu m^2$. Images of 10 randomly selected areas on the filter were taken to get an average cell count per image area, which was then multiplied by the total area of the filter to get the total number of cells collected on the in-line filter. A total of seven independent experiments with different starting cell cultures were carried out. The cells collected on the filter were assumed to be equal to the cells entering the impactor system. Fig. 2b shows a sample image of bacterial aerosol collected on a filter before the impactor entrance and stained with STYO 9. Fig. 2a is an image from $OD_{600} = 0.01$ PBS *E. coli* suspension and is shown for comparison. We can see that both Fig. 2a and b have a single layer of cells and can be therefore easily be counted.

3. Computational results

3.1. Gas flow field and particle dynamics

For the two-phase aerosol flow (air-bacteria) present in the impactor system, the equations for gas and particle dynamics are one-way coupled at low aerosol concentrations (Friedlander, 2000); the existence of aerosol has little effect on the gas while the aerosol flow is determined by the gas velocity. Therefore, the gas dynamics are solved independently using the Reynolds time-averaged Navier–Stokes equations shown in Cartesian tensor form:

$$\frac{\partial \rho}{\partial t} + \frac{\partial}{\partial x_j}(\rho v_j) = 0 \tag{2}$$

and

$$\frac{\partial}{\partial t}(\rho v_i) + \frac{\partial}{\partial x_j}(\rho v_i v_j) = -\frac{\partial p}{\partial x_i} + \frac{\partial}{\partial x_j}\left[\mu\left(\frac{\partial v_i}{\partial x_j} + \frac{\partial v_j}{\partial x_i} - \frac{2}{3}\delta_{ij}\frac{\partial v_l}{\partial x_l}\right)\right] + \frac{\partial}{\partial x_j}(-\rho\overline{v_i' v_j'}), \quad i = 1,2,3, \tag{3}$$

where ρ is the density, v is the velocity, p is the static pressure, δ is the Kronecker delta, μ is the viscosity, and i,j, and l are the cartesian indices. To close the form in Eq. (3), the Reynolds stress term $-\rho\overline{v_i' v_j'}$ is calculated using the Boussinesq hypothesis (Hinze, 1975). A standard $k-\varepsilon$ turbulence model is used in the gas flow equations.

The computational model details used to solve both gas and particle dynamics (flow and temperature) for the computational domain shown in Fig. 3 are discussed in our previous work (Sislian et al., 2009). In the current study, temperature effects are not analyzed. After obtaining the gas flow field, the particle trajectory is solved using Newton's second law:

$$m_p \frac{dv_p}{dt} = \frac{1}{2} C_D \rho_g A_p (v_g - v_p)|v_g - v_p|, \tag{4a}$$

$$\frac{dx}{dt} = v_p, \tag{4b}$$

where v_p and v_g are the velocity of the bacterial particle and gas, respectively, m_p is the mass of the particle, ρ_g is the density of the gas, A_p is the projected area of the bacterium on the plane perpendicular to the flow direction and C_D is the drag coefficient. The thermophoretic, gravitational and Basset history term are neglected in Eq. (4a). The drag force is assumed to be the major force acting on the bacterial particle which is typical for impactor systems. The bacterium is simulated as a 1 μm sphere with a density ρ_p of 1 mg/mL which is representative of values reported in literature (Laskin and Lechevalier, 1974; Willeke and Baron, 2001). All calculations are made to mimic the experimental conditions in the study with the $x/d = 1.2$ and both shock ($\chi = P_1/P_0 = 0.11, 0.50$) and non-shock ($\chi = 0.98$) conditions. The detailed conditions are shown in Section 3.3. The computational results provide predictions for bacterial envelope instability (see Section 3.2) and the collection efficiency of the impactor system at different operating conditions (see Section 3.3).

3.2. Bacterial envelope instability

The acceleration (or deceleration) of a bacterium relative to the gas phase creates instabilities in the bacterial envelope and break-up of the particle (Chandrasekhar, 1961; Joseph et al., 1999; Sislian et al., 2009). Specifically, waves are created on the bacterial surface perpendicular to the direction of acceleration (x-direction) which are stabilized by the bacterial surface tension. Under the assumption of viscous potential flow around a spherical cell, an estimate of the critical acceleration needed to overcome the stabilizing effect of surface tension can be computed using the derivation in (Joseph et al., 1999) (see also Chandrasekhar, 1961, Chapter 10) as follows:

$$a_c = 4\pi^2 \frac{\sigma}{\rho_p d_p^2} \tag{5}$$

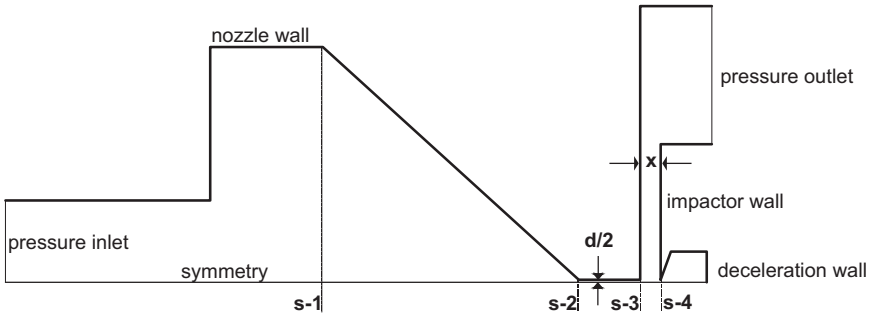

Fig. 3. Computational domain of the impactor. The dashed lines indicate different virtual surfaces. These surfaces are used to calculate the particle distribution at various cross-sections of the impactor shown as s-1, s-2, s-3 and s-4.

Table 1
Biological cell properties (Zinin et al., 2005) (not limited to bacteria) and critical shock properties needed to induce bacterial break-up.

Cell	d_p (μm)	σ (N/m)	a_c (m/s^2)	Oh	We_c
E. coli	1	7.5×10^{-3}	3.0×10^{8}	3.7×10^{-1}	1.4×10^{1}
D. carota	60	4.5×10^{1}	4.9×10^{8}	6.1×10^{-4}	1.2×10^{1}
M. hungatei	0.44	3.5–5	$0.7-1.0\times10^{12}$	$2.1-2.5\times10^{-2}$	1.2×10^{1}
C. eugametos	16	3.8×10^{1}	5.9×10^{9}	1.3×10^{-3}	1.2×10^{1}
B. emersonii	20	3.2×10^{1}	3.2×10^{10}	1.3×10^{-3}	1.2×10^{1}

where σ is the surface tension, ρ_p is the particle density and d_p is the particle diameter. Other sufficient conditions, which have to be satisfied for the critical acceleration to cause a break-up, are expressed in terms of two dimensionless numbers (Joseph et al., 1999). Specifically,

$$We > We_c = 12(1+1.077Oh^{1.6}), \tag{6a}$$

where

$$We = \frac{\rho_g(v_{p_i}-v_{g_i})^2 d_p}{\sigma} \tag{6b}$$

and

$$Oh = \frac{\mu_p}{(\rho_p d_p \sigma)^{1/2}} \tag{6c}$$

where *We* is the Weber number, which is the ratio between the inertial force exerted on the bacterial particle and the particle surface tension force. *Oh* refers to the Ohnesorge number, which is the ratio between the viscous forces and the surface tension force. v_{p_i} and v_{g_i} are the particle and gas velocity in the *x*-direction (i.e. direction of flow along centerline), respectively. We can therefore infer bacterial membrane break-up by computing the relative velocity $(v_{p_i}-v_{g_i})$ of the bacterium, as well as the maximum acceleration achieved. The criteria that both deceleration and Weber number have to be above the critical values are sufficient for the bacterial cell to break-up as they pass through the shock. However, if only the Weber number is above its critical value the cells may experience membrane vibrations, boundary layer stripping, or even break-up (Joseph et al., 1999). Furthermore, the model does not account for loss of viability without break-up which is a more stringent requirement than other mechanisms.

Bacterial cells with a lower surface tension and larger diameters require lower accelerations to break-up. It is important to note that the surface tension values reported in Table 1 are derived from the turgor pressure (Zinin et al., 2005). However, the surface tension can vary with deformation generated by fluid flow over the cell membrane. Such a variation of the cell surface tension under fluid flow may limit the accuracy of the critical acceleration predictions of Table 1. In such a case, more accurate models of the variation of cell surface tension under stress generated by the fluid flow (similar to the works of Kleinig and Middelberg, 1996, 1998; Smith et al., 1998; Zhang et al., 1992) should be utilized and combined with the fluid flow and particle motion models developed here to make accurate critical acceleration predictions. We also note that previous work (Kleinig and Middelberg, 1998) has demonstrated for the first time the use of inertial forces (expressed in terms of the Weber number and acceleration) in achieving cell break-up in the context of a high-pressure homogenization system. As shown in Table 1, vegetative cells represented by *E. coli* require critical accelerations (a_c) of 3.0×10^8 m/s^2. On the other hand, spores represented by *M. hungatei*, an archea, require accelerations of about four orders of magnitude more than vegetative cells. In our previous parametric study of the impactor system (Sislian et al., 2009) where P_1, P_0 and x/d were varied, it was shown that we can achieve accelerations on the order of 10^9-10^{10} m/s^2 in our current system operating under shock conditions. Break-up of spores using the current impactor geometry is not possible. Furthermore, it is possible to achieve accelerations below 10^8 m/s^2 by operating the impactor at non-shock conditions.

A shock is represented as a sharp discontinuity in fluid properties (velocity, temperature, pressure) and can be seen in Fig. 4a. Due to its inertia, a bacterial particle is not able to follow the sharp drop in gas velocity and will therefore experience a relative deceleration of 4.95×10^9 m/s^2 at $\chi=0.11$ and 2.02×10^8 m/s^2 at $\chi=0.50$ (both above the critical acceleration of *E. coli*). However, in the non-shock condition with $\chi=0.98$ (see Fig. 4b) the gas properties do not experience sharp changes. In the incompressible flow the gas decelerates because of the larger area due to the expansion after exiting the nozzle. The bacterial particle is, therefore, able to adjust to the gas velocity and experience a much lower relative deceleration of 3.89×10^6 m/s^2. The deceleration of the bacterial particle in the non-shock case is not large enough ($<3.0\times10^8$ m/s^2, see Table 1) to cause the break-up of the cell envelope. Fig. 4c and d shows the acceleration of the bacterial particle as a function of the distance from the exit

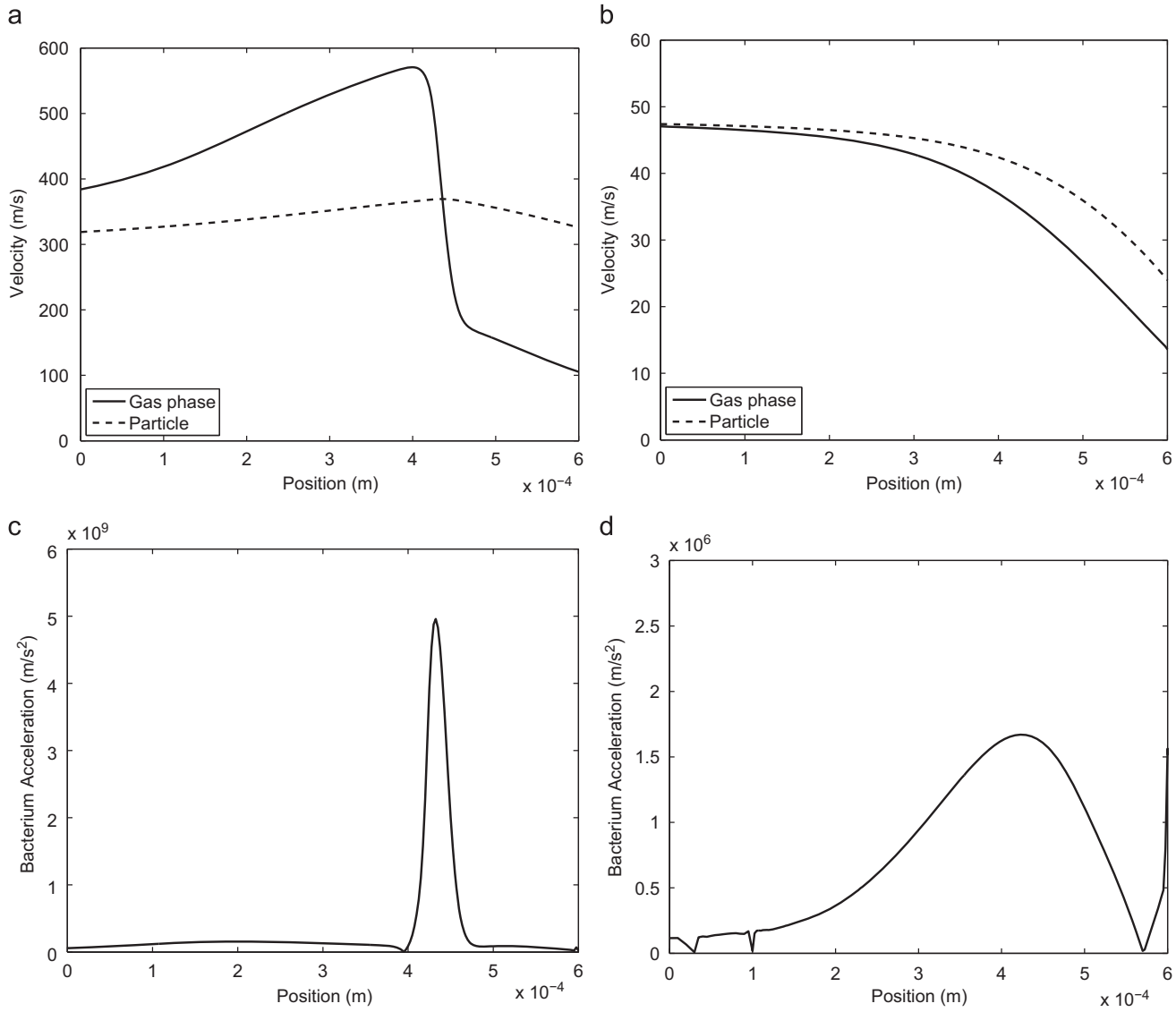

Fig. 4. (a, b) Centerline particle and gas velocity and (c, d) bacterial particle acceleration (relative to gas flow) as a function of the distance from the nozzle. The entrance of the collection tube is at a distance 6×10^{-4} m from the nozzle exit. Impactor operating conditions: (a, c) $\chi = 0.11$ and (b, d) $\chi = 0.98$.

of the nozzle. In the shock case with $\chi = 0.11$, the peak acceleration lasts for a short distance and is three orders of magnitude larger than the non-shock case. We therefore operated the impactor system at both the shock ($\chi = 0.11, 0.50$) and non-shock ($\chi = 0.98$) conditions to obtain, in addition to the computational data, experimental bacterial viability data (see Section 4).

Remark 1. At $\chi = 0.98$, the acceleration of the bacterial particle shown in Fig. 4d experiences a sharp change at a position greater than 0.55 mm from the exit of the nozzle. The change is because of the stagnant gas at the entrance of the deceleration tube, especially since Brownian motion is neglected in these calculations. The maximum acceleration is calculated at a position approx. 0.4 mm from the nozzle.

Remark 2. The particle accelerations were calculated by tracking a bacterium released on the centerline of the impactor, where the aerodynamic shock has the highest Mach number. Therefore, the calculated bacterial accelerations represent a maximum in a distribution if the particle accelerations were to be calculated at all points. These off-centerline accelerations can represent values lower than the critical value of 3.0×10^8 m/s^2 required to break-up the *E. coli* cells. In the experiments, the *E. coli* cells will experience the distribution of accelerations. Therefore, we do not expect all cells to lose viability, especially since they pass the shock at different points as explained in Section 3.3.

3.3. Bacterial collection efficiency in the impactor

The collection efficiency (η) is defined as the number of particles that pass through the collection tube entrance versus the number of particles that enter the impactor inlet. The bacterial collection efficiency (η) for all three impactor operating conditions ($\chi = 0.11, 0.50, 0.98$) are evaluated to determine the overall bacterial aerosol neutralization rate in Section 4. For a highly turbulent flow (see Fig. 5a and b) and low-density, small-size aerosols, particle dispersion due to gas velocity fluctuations could be significant and should be accounted for in the calculation of

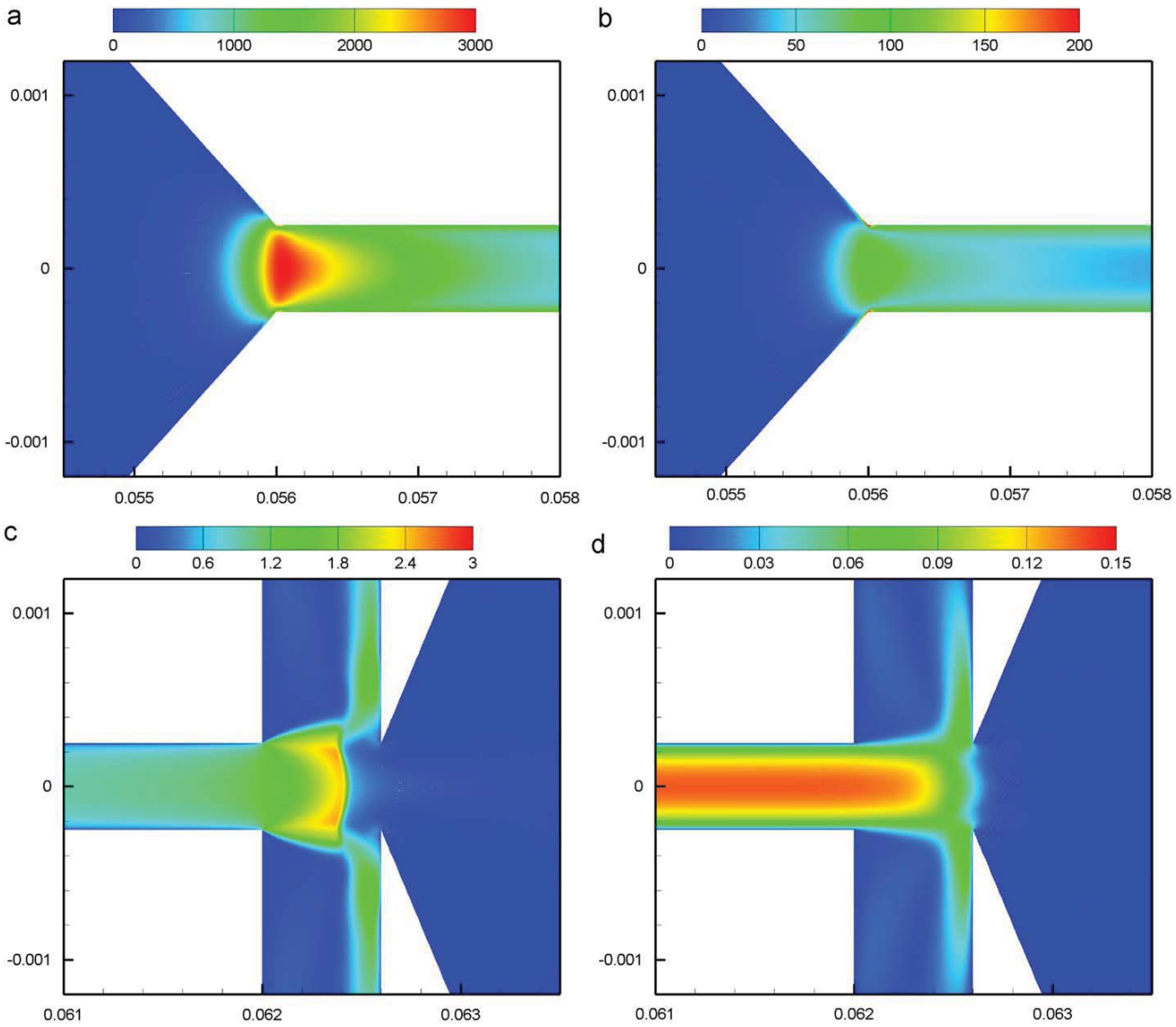

Fig. 5. (a, b) Turbulent kinetic energy (m^2/s^2) contours of the gas phase in the converging region of the nozzle. A region of high turbulence can be seen in the converging part. (c, d) Mach contours at the exit of the nozzle. Conditions: (a, c) shock with $\chi = 0.11$ and (b, d) non-shock with $\chi = 0.98$. Note that the scales are different for the different conditions.

collection efficiency. The gas dynamics, described in Section 3.1, is based on a turbulent model and only provides a Reynolds-averaged velocity while the velocity fluctuation terms are not explicitly described. The random walk model is employed in this work to study the effect of velocity fluctuation on bacterial aerosol with reasonable computational load. Stochastic tracking of the particles is used in order to account for the turbulence dispersion effects of the gas flow. In Section 3.2, the average values of the gas velocity were used to evaluate the maximum relative acceleration of the particles on the centerline. In the stochastic tracking model, however, the gas velocity is represented as an average plus a fluctuating term when calculating the particle velocity, v_p, in Eq. (4a). The fluctuating velocity is kept constant for time intervals corresponding to the lifetime of the eddies. The following equations describe the stochastic behavior:

$$v_g = \overline{v} + v', \tag{7a}$$

$$v' = \zeta\sqrt{\overline{v'^2}} = \zeta\sqrt{2k/3}, \tag{7b}$$

$$t_L = 0.15\,k/\varepsilon, \tag{7c}$$

$$\tau_\varepsilon = -t_L \log r, \tag{7d}$$

where v_g is the instantaneous gas velocity, $\overline{v}$ is the average velocity and v' is the velocity fluctuation term. v' is a function of ζ, a normally distributed random number, and $\overline{v'^2}$ is the local root mean square of the fluctuations. $\overline{v'^2}$ is calculated based on the assumption of isotropy and is given by $\overline{v'^2} = 2k/3$, with k being the turbulence kinetic energy in the $k-\varepsilon$ model. Finally, t_L is the Lagrangian time interval, ε is the turbulence dissipation rate, τ_ε is the lifetime of the eddies, and r is a uniformly distributed random number between 0 and 1. Fig. 6 shows the path of five particles released from the inlet as they exit the nozzle of the impactor system for both $\chi = 0.11$ (Fig. 6a) and $\chi = 0.98$ (Fig. 6b). In

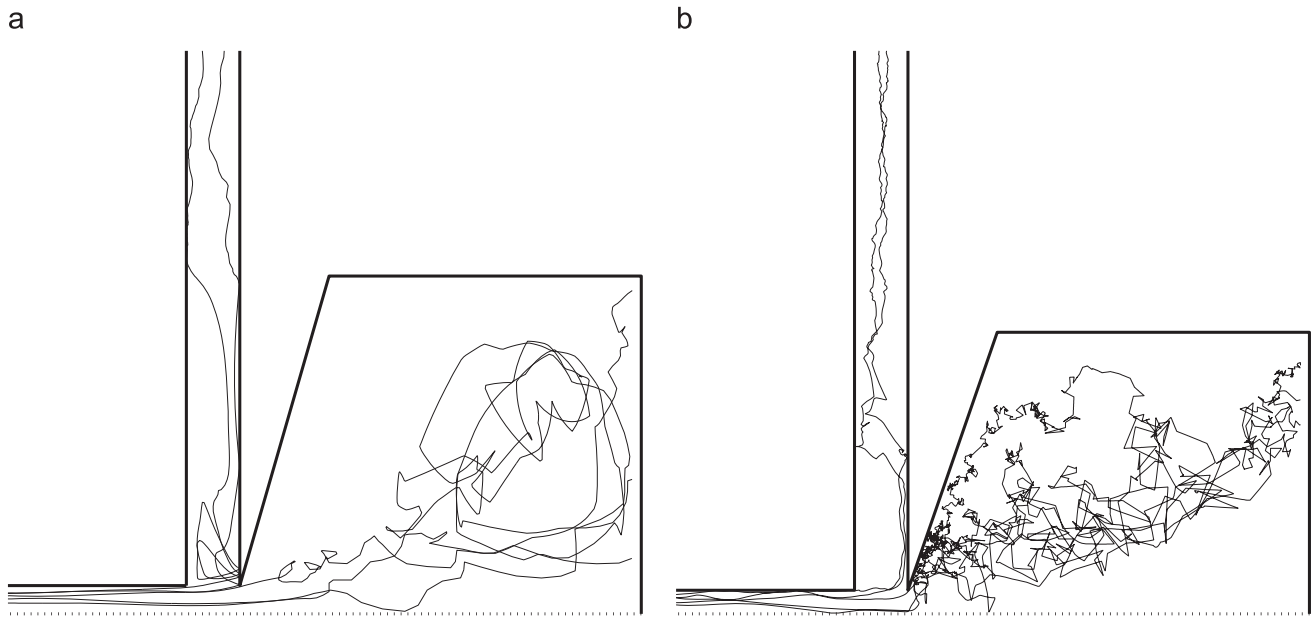

Fig. 6. Representative trajectories of five particles released from the inlet of the impactor for both (a) $\chi = 0.11$ and (b) $\chi = 0.98$. The collection efficiencies as measured by the number of particles entering the collection tube are 0.51 and 0.36 for $\chi = 0.11$ and $\chi = 0.98$, respectively. (Note that a different scale (even though the physical domain is the same) is used in the plots to present particle trajectories in the left plot more clearly.)

Table 2
Critical parameters for different operating conditions with $x/d = 1.2$.

P_0 (atm)	$\chi(=P_1/P_0)$	$a_{\max}$ (m/s^2)	We_{max}	M_{max}	Re	η
1.0	0.98	1.67×10^6	1.7×10^{-2}	0.13	9.9×10^2	0.35
1.0	0.50	2.02×10^8	3.5×10^0	0.96	5.8×10^3	0.72
1.0	0.11	4.96×10^9	3.1×10^0	2.36	5.4×10^3	0.51
5.0	0.11	5.98×10^9	1.5×10^1	2.32	3.2×10^4	0.38

calculating η, 10,000 particles are released at the inlet of the impactor. The particles are then counted as they pass the different virtual surfaces shown in Fig. 3 as s-1, s-2, s-3 (nozzle exit) and s-4 (deceleration tube entrance) (see Remark 3). All the boundaries shown in Fig. 3, except pressure inlet and pressure outlet, are assumed to be reflection boundaries. The collection efficiency is defined as follows:

$$\eta = \frac{n_c'}{n_i}, \tag{8}$$

where n_i is the number of particles entering the impactor (see also Remark 3) and n_c' is the number of particles that enter the collection tube. n_c' is calculated under the assumption of no break-up. η is used to determine the total number of live cells that would be collected if the shock were to have no effect (see Section 4.2). For different operating conditions, the collection efficiency (η) is reported in Table 2. The maximum acceleration (a_{max}) and Weber number (We_{max}), which enable the prediction of the experimental break-up, are also reported in Table 2. The critical acceleration conditions that satisfy the requirements for break-up as discussed in Section 3.2 are met for $\chi = 0.11$ and 0.50; however, the conditions for the Weber number are not. Increasing the upstream pressure to 5 atm will increase the We to 15 while keeping the maximum acceleration similar as shown in Table 2. However, as reported in Section 4.2, cells will still break-up under non-critical Weber number conditions. The Reynolds number at the exit of the nozzle and the maximum Mach number of the gas are also reported to give insight into the flow characteristics of the impactor. The effect of these different conditions is described in detail in Section 4.

Remark 3. Despite the reflective boundary conditions employed in the simulations, not all 10,000 particles released from the inlet of the impactor are accounted for at the exit of the nozzle (Fig. 3; s-3). For $\chi = 0.11$, 0.50 and 0.98 only 7,763, 9840 and 9500 particles are counted, respectively. For $\chi = 0.11$ and 0.50, 10^5 integration steps were used to calculate the particle track. For $\chi = 0.98$, 2×10^5 and 4×10^5 integration steps were used; in the first case 3840 particles were counted and in the second 9500. Both integration steps resulted in a collection efficiency of 0.35. Therefore, in the calculation of collection efficiency the number of particles exiting the nozzle are assumed to be the total number of particles entering the impactor.

Remark 4. Fig. 7 shows the particle distribution at different surfaces (s-1, s-2, s-3 and s-4) of the impactor system. The particle distribution at the entrance of the collection tube is shown in Fig. 7g and h, where the dotted line indicates the edge of the entrance. In the $\chi = 0.98$ case, the peak occurs away from the center and this can be expected for $x/d < 4$ according to Burwash et al. (2006). Similar distributions have also been observed by other researchers (Abouali and Ahmadi, 2005; Sethi and John, 1993). The particle distribution in the shock condition has a peak at the center of the collection tube entrance.

4. Cell viability results and discussion

Quantitative experimental measurements of cell viability were obtained via fluorescence flow cytometry (see Section 4.1) and fluorescence microscopy (see Section 2.4). Experimental data are supplemented with computational data on the collection efficiency of the impactor (see Section 3.3) for the different operating conditions. The goal is to assess the fraction of cells that remain alive after the effect of impactor operation (f_l):

$$f_l = \frac{n_c}{n_c'}, \tag{9}$$

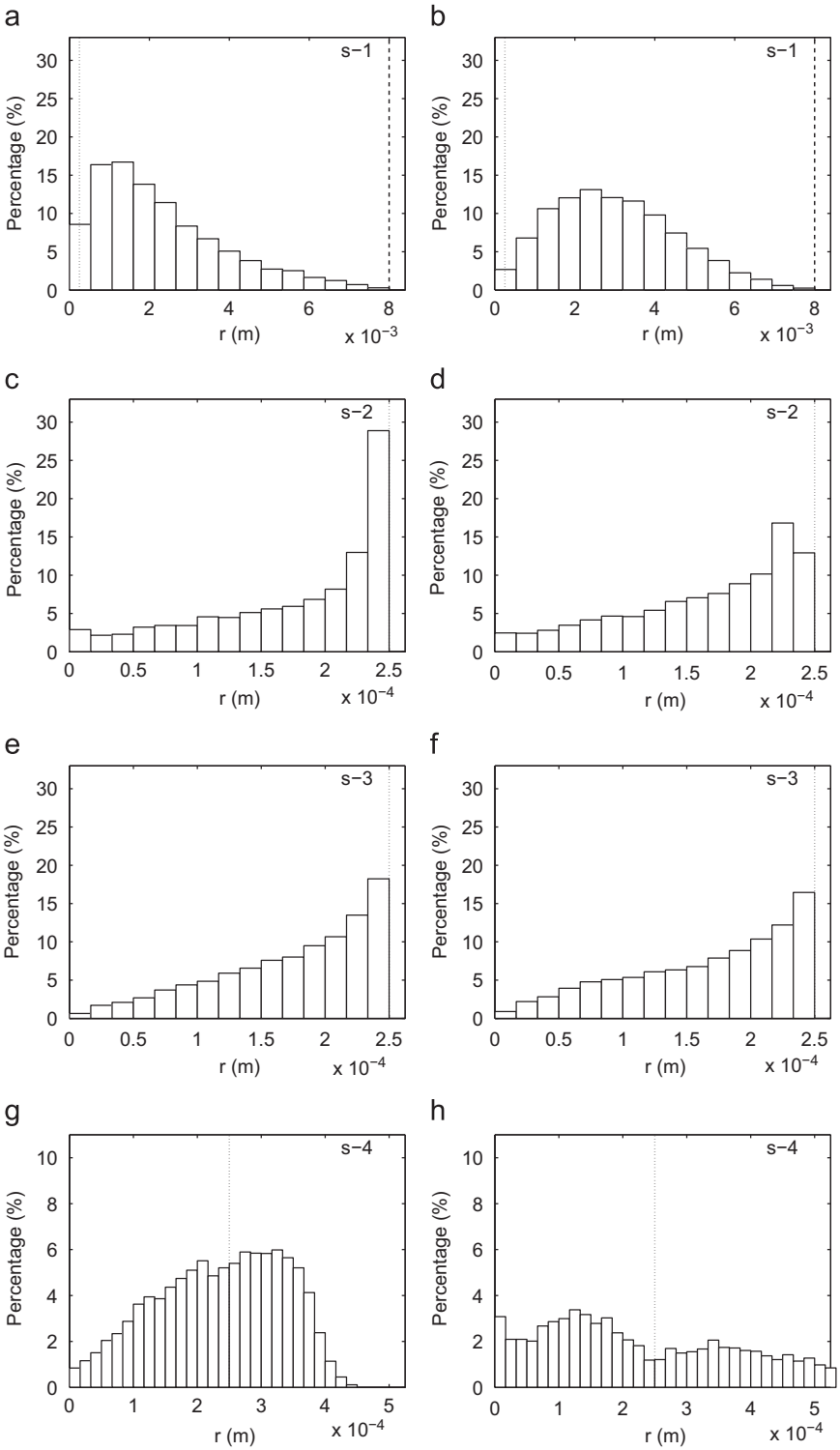

Fig. 7. Distribution of particles along different surfaces (s-1, s-2, s-3, s-4) labeled in the Fig. 3. The *x*-axis is the distance (r) in meters from the centerline and the *y*-axis is the percentage of total particles released from the inlet of the impactor. The dashed and dotted lines indicate the wall of the impactor at s-1, s-2 and s-3, respectively. At s-4 the dotted line indicates the entrance of the collection tube. (Left plots) Particles released under shock conditions and (right plots) particles released under non-shock conditions.

where n_c is the experimentally measured number of live cells including the break-up model and n_c' is the number of live cells that enter the collection tube under the assumption of no break-up (i.e. all cells are alive—see Eq. (11)). f_l for the different operating conditions will be compared to assess the effect of the aerodynamic shock on the bacterial aerosol. The following sections will detail the data used to calculate f_l.

4.1. Fluorescence cytometry

The experimental fluorescence cytometry protocol described in Section 2.3 is used to obtain the data shown in Fig. 8. The data shown in Fig. 8 represents one set of experiments. A total of 15 sets of experiments were conducted, each from a different starting cell culture, to obtain statistically significant results in the calculation of f_l.

The left dot-plots in Fig. 8 represent the side-scatter (y-axis) and forward-scatter (x-axis) of a particle passing the laser beam in the flow cytometer. Each dot represents a particle's side and forward scatter intensities. The side scatter is a measure of the granularity and complexity while the forward scatter is related to the surface area (i.e. size) of the particle. The population of bacterial particles, enclosed in the gate denoted by G2/G3 in Fig. 8, is determined by running a PBS only solution to isolate the background enclosed in the gate denoted by G1. The right dot-plots shows the red fluorescence (FL2-H) versus green fluorescence (FL1-H) intensity for the gated (i.e. inside the polygon G2/G3) cell population. The analysis of the fluorescence plots provides information on the viability of the cell population. In Fig. 8d the EtOH cell population can clearly be seen to lie in the top left half denoted by D. Live cells can be counted in the bottom right half denoted by L. Similar patterns have also been observed in the literature (Berney et al., 2007). Furthermore, Berney et al. (2007) indicate the presence of an intermediate state where the outer membrane in gram-negative cells is compromised. The intermediate state population can be seen as the population with the highest intensity green fluorescence in the L gate. For the purposes of the current study, the intermediate state cell population is grouped with the live population in order to make the requirements for neutralization more stringent.

The fraction of live cells (cells in bottom right half divided by total gated cells or $L/(L+D)$) in all analyzed samples is shown in Fig. 9. The error bars are the 95% confidence interval limits on the data using a normal fit. The data does not take into account the mass balance on the system to indicate the overall neutralization rate. The data as shown in Fig. 9 ignores the break-up of cells since only intact cells are analyzed. Therefore, only a mass balance on the overall system can lead to the determination of the overall cell neutralization rate $(1-f_l)$ or f_l. However, Fig. 9 provides raw data on the collected samples.

The percentage of live cells in the nebulized sample can differ from that in the suspension because of the operating conditions of the nebulizer. The data in Fig. 9a, represents five experiments with different starting cultures. The fraction of live cells in the suspension (0.910 ± 0.014) is equal to that of the nebulization (0.938 ± 0.005) with $p > 95\%$ using a two tailed t-test with unequal variance. Therefore, the effect of nebulization can be neglected in the calculation of the neutralization rate.

In Fig. 9b, fifteen experiments with different starting cultures were conducted for each of the operating conditions of the impactor. Both shock conditions ($\chi = 0.11$ and 0.50) have statistically equal fraction of live cells while they are lower statistically from the non-shock condition ($\chi = 0.98$). The cells exposed to ethanol (positive control) have the lowest fraction of live cells.

4.2. Mass balance

To evaluate the effect of particle acceleration in an aerodynamic shock a mass balance on the entire experimental system has to be done to account for all losses. Bacterial aerosol is lost to the walls of the system between the exit of the nebulizer and the entrance of the impactor. Determining the losses is important in

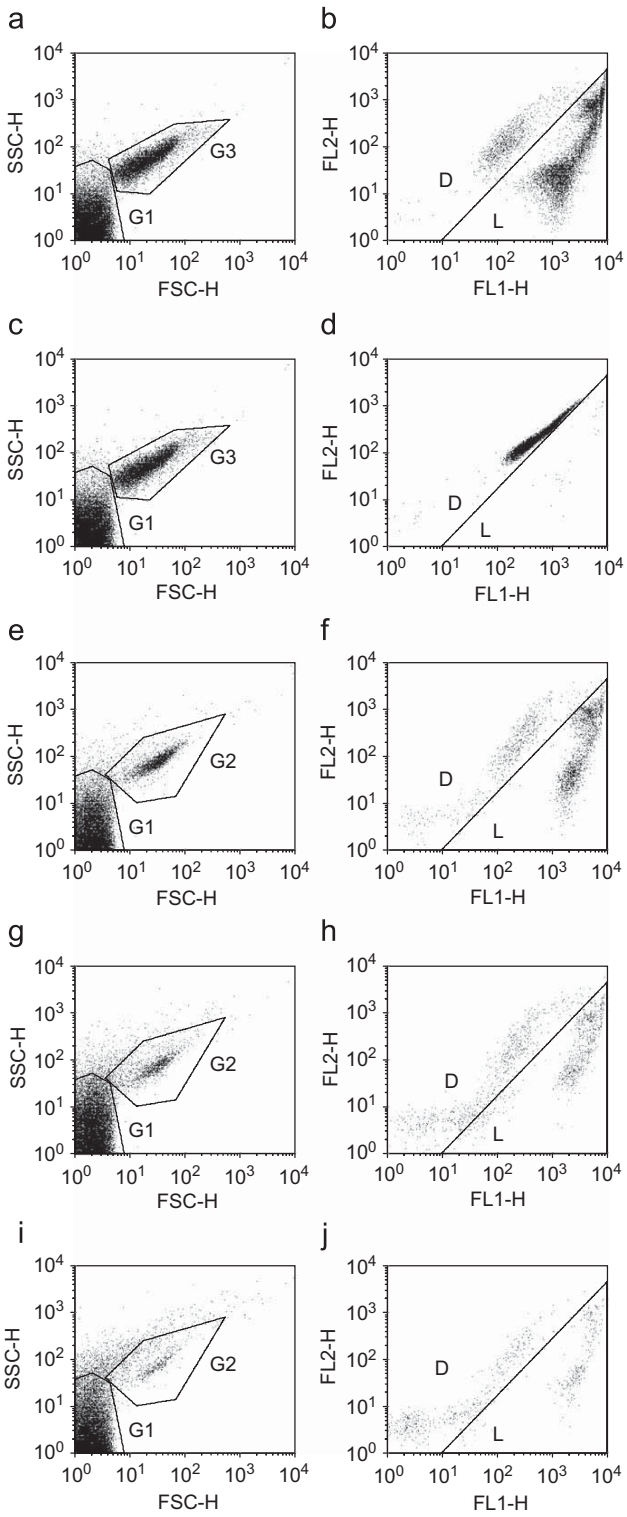

Fig. 8. (Left) Side-scatter versus forward-scatter plot of all particles in the flow cytometer. The G2/G3 gate indicates the particle sizes which represent intact cells. G1 indicates the debris population. (Right) Red fluorescence (FLH-2) versus green fluorescence (FLH-1) of gated cells in the left side plots. The L gate represents the live cells and the D gate represents the dead cells. (a, b) Cell suspension in PBS, (c, d) cell suspension in EtOH, (e, f) cells collected after passing impactor operated at $\chi = 0.98$, (g, h) $\chi = 0.50$ and (i, j) $\chi = 0.11$.

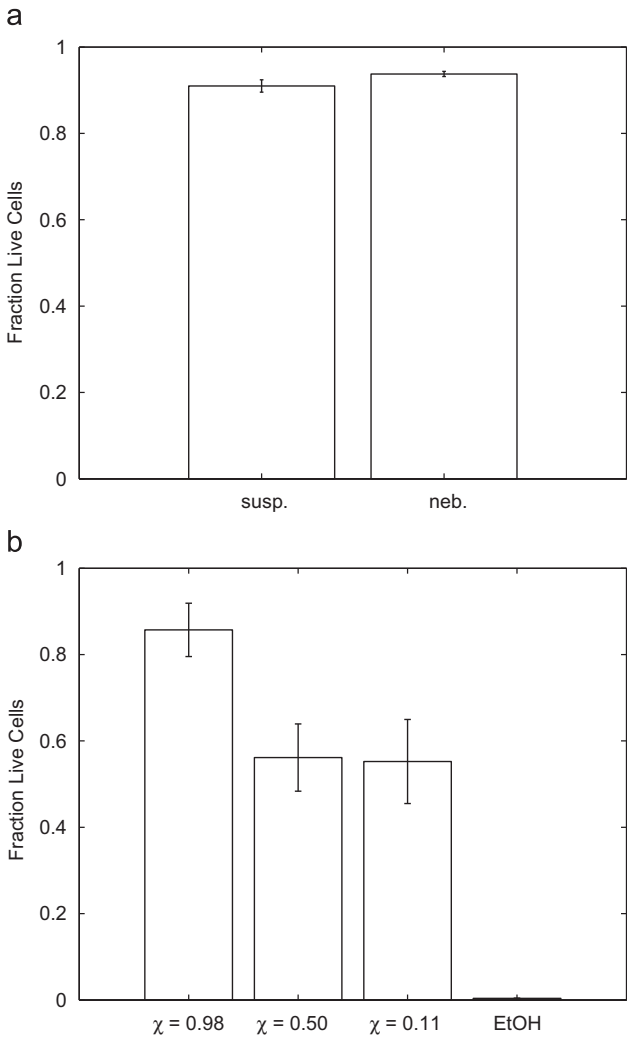

Fig. 9. Fraction of live cells in different collected samples. (a) All experiments start with a measurement of the fraction of live cells in the cell culture (susp), the negative control and in the nebulized cells (neb). Error bars show the 95% confidence interval using a normal distribution for five measurements per sample. (b) The cells that pass through the impactor system and then collected in the collection tube at $\chi = 0.98$, $\chi = 0.50$ and $\chi = 0.11$ with $P_0 = 1$ atm. The ethanol (EtOH) suspension is the positive control. Error bars show the 95% confidence interval using a normal distribution for 15 measurements per sample.

the overall neutralization rate and is calculated as follows:

$$\phi = \frac{n_n}{n_i}, \tag{10}$$

where n_n is the total number of cells that are nebulized and n_i is the total number of cells that enter the impactor. Experimental measurements (see Section 2.4) determine the actual number of particles that enter the impactor after losses in the nebulization process and in the tubes connecting the nebulization chamber to the impactor inlet. The measured ϕ is 0.088 ± 0.029 for all operating conditions of the impactor system. Losses to the walls of the nozzle after the impactor entrance are neglected. Nonetheless, not all the particles that enter the impactor are collected for analysis as detailed in Section 4.1. By assuming no cell break-up, we can calculate the number of live cells that enter the collection tube (n_c') as

$$n_c' = n_{sl}\phi\eta, \tag{11}$$

where n_{sl} is the number of live cells imputed to the system by nebulizing the suspension and is obtained experimentally by counting the cells in the lower right half (L) of Fig. 8b. The collection efficiency of the impactor for the different operating conditions is listed in Table 2. Eq. (9) then becomes

$$f_l = \frac{n_c}{n_{sl}\phi\eta}, \tag{12}$$

where n_c is obtained by counting the number of cells in the lower right half (L) of Fig. 8f or equivalent data for the different impactor operating conditions (Fig. 8h and j).

4.3. Effect of the aerodynamic shock

By combining fluorescence cytometry, microscopy and computational collection efficiencies in Eq. (12), we can obtain the values for f_l for the different operating conditions in the impactor system. The data is shown in Fig. 10 with the 95% confidence interval on the normal fit of fifteen independent experiments for each condition and using error propagation. In the experimental impactor system operating at $\chi = 0.98$, the bacterial aerosol does not experience the critical acceleration discussed in Section 3.2; therefore, the f_l is an order of magnitude higher than the conditions which lead to acceleration greater than the critical ($> 3.00 \times 10^8\,\mathrm{m/s^2}$). The acceleration at $\chi = 0.50$ is $2.02 \times 10^8\,\mathrm{m/s^2}$ which is approximately equal (considering experimental variation in pressure and assumptions in calculating the computational accelerations mention in Section 3) to the critical acceleration. In this case, a reduction in cell viability can be seen that is statistically the same as that observed for $\chi = 0.11$ with an acceleration of $4.96 \times 10^9\,\mathrm{m/s^2}$.

It is important to note that the Weber numbers in Fig. 10 for $\chi = 0.11$, 0.50 and 0.98 carried at $P_0 = 1$ atm are in the range $[0.0017, 3.5]$ (see Table 2) which is lower than the computational model-predicted critical Weber number of 14 needed for bacterial break-up. However, Fig. 10 clearly demonstrates that this estimate is conservative and an order of magnitude reduction in cell viability can be attained at a lower Weber number than 14 if the critical acceleration is achieved. To investigate this point further, we carried out experiments (see Remark 5) at a Weber

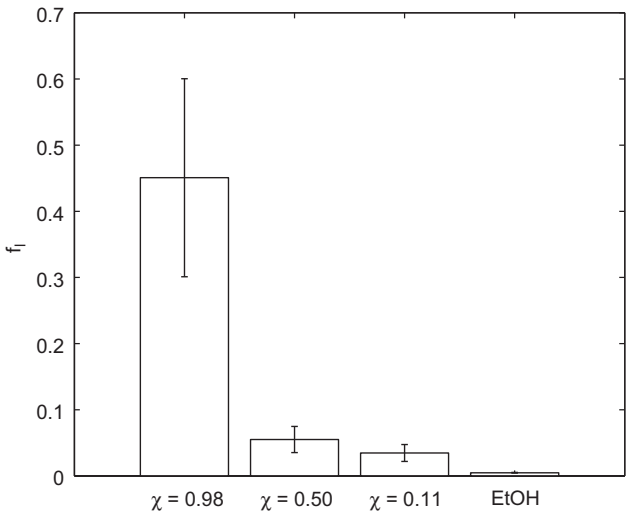

Fig. 10. Fraction of cells that remain alive after the effect of impactor operation (f_l) and after exposure to ethanol. Live cells in these samples are compared to live cells in the negative control by accounting for losses before the impactor and for the collection efficiency of the impactor. Error bars show the 95% confidence interval using a normal distribution for 15 measurements per sample.

number of 15 and an acceleration of 5.98×10^9 (both in the range needed for bacterial break-up) with $\chi = 0.11$ at $P_0 = 5$ atm and found no statistical difference in fraction of cells remaining live ($f_l = 0.047 \pm 0.016$ at $P_0 = 5$ atm compared to $f_l = 0.035 \pm 0.012$ at $P_0 = 1$ atm). Therefore, the sharp decelerations that the cells experience after they pass through the shock is the main reason for which they lose viability.

Remark 5. Five experiments were carried out at a higher upstream pressure, $P_0 = 5$ atm ($We = 15$), to investigate the influence of Weber number on cell viability. In order to run the impactor system of Fig. 1 at an upstream pressure of $P_0 = 5$ atm, a high pressure chamber was designed to encase the nebulizer, and the HEPA filter was removed to avoid exposure to atmospheric pressure before the impactor. Furthermore, the nebulizer was operated at $P_n = 10$ atm to maintain the same P_n/P_0 ratio as the atmospheric pressure experiments. The bends in the tubing connecting the nebulizer to the impactor were also modified; this modification might slightly change the losses as measured by ϕ; however, in our calculations we assumed the losses as calculated in Section 4.2 stayed constant for all experiments. All other conditions were maintained as described in Section 2. The fraction of live cells in the collection tube in these five experiments was found to be 0.332 ± 0.215 and the corresponding f_l was computed to be $f_l = 0.047 \pm 0.016$.

5. Conclusions

Neutralization of bacterial aerosols using aerodynamic shocks is important in countering bioterrorism. The computational model developed in our previous study (Sislian et al., 2009) was validated by experimental viability analysis on vegetative gram-negative *E. coli* cells. The *E. coli* cells were used as a model bacterial aerosol with a computational-model predicted critical acceleration of 3.0×10^8 m/s^2 to achieve bacterial break-up. The experimental impactor system was operated under three conditions to provide maximum accelerations of 4.96×10^9, 2.02×10^8 and 1.67×10^6 m/s^2; values above, equal and below the predicted critical acceleration for *E. coli*, respectively. The experiments show that for accelerations higher than the critical value the shock has a considerable effect, $f_l = 0.055 \pm 0.020$ for $\chi = 0.50$ and $f_l = 0.035 \pm 0.012$ for $\chi = 0.11$. Under the non-shock condition, $f_l = 0.451 \pm 0.150$ which is an order of magnitude higher survival rate than that found at higher accelerations. These results confirm the computational model predictions. The computational model can therefore be used to predict the effect of an aerodynamic shock on bacterial cells given their surface tension and size. The Weber number seems to have little effect on the break-up of cells. In future work, we will explore the effect of the shock on other bacterial cells.

Notation

a_c	critical bacterial acceleration
A_p	projected area of particle
C_D	drag coefficient
d	nozzle diameter
d_p	particle diameter
f_l	fraction of cells that remain alive after the effects of acceleration
k	turbulent kinetic energy
m_p	particle mass
n_c	experimentally measured number of live cells
n_c'	number of live cells under assumption of no break-up
n_i	number of particles entering the impactor
n_n	number of cells nebulized
n_{sl}	number of cells live after nebulization
Oh	Ohnesorge number
p	static pressure of gas
P_0	upstream stagnation pressure
P_1	downstream stagnation pressure
P_n	nebulization pressure
t_L	Lagrangian time interval
v/v_g	gas velocity
v_p	particle velocity
We	Weber number
We_c	critical Weber number
x	plate to nozzle distance
Greek letters	
γ	heat capacity ratio
ε	rate of turbulent dissipation
ζ	normally distributed random variable
η	impactor collection efficiency
μ/μ_g	dynamic viscosity of gas
ρ/ρ_g	gas density
ρ_p	particle density
σ	bacterial surface tension
τ_ε	lifetime of eddies
ϕ	fraction of particles not lost before entering impactor
χ	downstream to upstream pressure ratio

Acknowledgments

This work has been supported by the Defense Threat Reduction Agency (DTRA) under Grant number HDTRA1-07-0012. The authors would like to acknowledge the late Prof. Sheldon K. Friedlander for initiating the project and for advising Patrick R. Sislian at the early stage of his work. The authors would also like to thank Prof. Jennifer A. Jay for providing unrestricted access to the fluorescence microscope. Flow cytometry was performed in the UCLA Jonsson Comprehensive Cancer Center (JCCC) and Center for AIDS Research Flow Cytometry Core Facility that is supported by National Institutes of Health awards CA-16042 and AI-28697, and by the JCCC, the UCLA AIDS Institute, and the David Geffen School of Medicine at UCLA.

References

Abouali, O., Ahmadi, G., 2005. A model for supersonic and hypersonic impactors for nanoparticles. Journal of Nanoparticle Research 7 (1), 75–88.

Alvi, F.S., Ladd, J.A., Bower, W.W., 2002. Experimental and computational investigation of supersonic impinging jets. AIAA Journal 40 (4), 599–609.

Berney, M., Hammes, F., Bosshard, F., Weilenmann, H.U., Egli, T., 2007. Assessment and interpretation of bacterial viability by using the live/dead BacLight kit in combination with flow cytometry. Applied and Environmental Microbiology 73 (10), 3283–3290.

Biswas, P., Flagan, R.C., 1988. The particle trap impactor. Journal of Aerosol Science 19 (1), 113–121.

Bovallius, A., Bucht, B., Roffey, R., Anas, P., 1978. Three-year investigation of natural airborne bacterial-flora at four localities in Sweden. Applied and Environmental Microbiology 35 (5), 847–852.

Burwash, W., Finlay, W., Matida, E., 2006. Deposition of particles by a confined impinging jet onto a flat surface at $Re = 10^4$. Aerosol Science and Technology 40 (3), 147–156.

Chandrasekhar, S., 1961. Hydrodynamic and Hydromagnetic Stability, The International Series of Monographs on Physics first ed Clarendon Press, Oxford.

Delamora, J.F., Hering, S.V., Rao, N., McMurry, P.H., 1990a. Hypersonic impaction of ultrafine particles. Journal of Aerosol Science 21 (2), 169–187.

Delamora, J.F., Rao, N., McMurry, P.H., 1990b. Inertial impaction of fine particles at moderate Reynolds-numbers and in the transonic regime with a thin-plate orifice nozzle. Journal of Aerosol Science 21 (7), 889–909.

Di Giorgio, C., Krempff, A., Guiraud, H., Binder, P., Tiret, C., Dumenil, G., 1996. Atmospheric pollution by airborne microorganisms in the city of marseilles. Atmospheric Environment 30 (1), 155–160.

Friedlander, S.K., 2000. Smoke, Dust, and Haze: Fundamentals of Aerosol Dynamics, Topics in Chemical Engineering second ed Oxford University Press, Oxford.

Hering, S.V., Flagan, R.C., Friedlander, S.K., 1978. Design and evaluation of new low-pressure impactor. 1. Environmental Science & Technology 12 (6), 667–673.

Hering, S.V., Friedlander, S.K., Collins, J.J., Richards, L.W., 1979. Design and evaluation of a new low-pressure impactor. 2. Environmental Science & Technology 13 (2), 184–188.

Hinze, J.O., 1975. Turbulence, McGraw-Hill Series in Mechanical Engineering second ed McGraw-Hill, New York.

Horneck, G., Stoffler, D., Eschweiler, U., Hornemann, U., 2001. Bacterial spores survive simulated meteorite impact. Icarus 149 (1), 285–290.

Joseph, D.D., Belanger, J., Beavers, G.S., 1999. Breakup of a liquid drop suddenly exposed to a high-speed airstream. International Journal of Multiphase Flow 25 (6–7), 1263–1303.

Jurcik, B.J., Brock, J.R., Trachtenberg, I., 1989. A study of low-pressure particle impaction processes. Journal of Aerosol Science 20 (6), 701–711.

Kleinig, A.R., Middelberg, A.P.J., 1996. The correlation of cell disruption with homogenizer valve pressure gradient determined by computational fluid dynamics. Chemical Engineering Science 51 (23), 5103–5110.

Kleinig, A.R., Middelberg, A.P.J., 1998. On the mechanism of microbial cell disruption in high-pressure homogenisation. Chemical Engineering Science 53 (5), 891–898.

Laflamme, C., Lavigne, S., Ho, J., Duchaine, C., 2004. Assessment of bacterial endospore viability with fluorescent dyes. Journal of Applied Microbiology 96 (4), 684–692.

Laskin, A.I., Lechevalier, H.A., 1974. CRC Handbook of Microbiology, vol. 1. CRC Press, Boca Raton, FL.

Liepmann, H.W., Roshko, A., 2001. Elements of Gas Dynamics, Dover Books on Engineering. Dover Publications.

Lighthart, B., Shaffer, B.T., 1997. Increased airborne bacterial survival as a function of particle content and size. Aerosol Science and Technology 27 (3), 439–446.

Lundbeck, H., Skoldber, O., 1963. Effect of pressure waves on bacteria suspended in water. Biotechnology and Bioengineering 5 (3), 167–184.

Mancinelli, R.L., Shulls, W.A., 1978. Airborne bacteria in an urban environment. Applied and Environmental Microbiology 35 (6), 1095–1101.

Powell, A., 1988. The sound-producing oscillations of round underexpanded jets impinging on normal plates. Journal of the Acoustical Society of America 83 (2), 515–533.

Sethi, V., John, W., 1993. Particle impaction patterns from a circular jet. Aerosol Science and Technology 18 (1), 1–10.

Shapiro, A.H., 1953. The Dynamics and Thermodynamics of Compressible Fluid Flow. The Ronald Press Company, New York.

Sislian, P.R., Zhang, X., Li, M., Pham, D., Mädler, L., Christofides, P.D., 2009. Bacterial aerosol neutralization by aerodynamic shocks using a novel impactor system: design and computation. Chemical Engineering Science 64 (9), 1953–1967.

Smith, A.E., Moxham, K.E., Middelberg, A.P.J., 1998. On uniquely determining cell-wall material properties with the compression experiment. Chemical Engineering Science 53 (23), 3913–3922.

Stewart, S.L., Grinshpun, S.A., Willeke, K., Terzieva, S., Ulevicius, V., Donnelly, J., 1995. Effect of impact stress on microbial recovery on an agar surface. Applied and Environmental Microbiology 61 (4), 1232–1239.

Teshima, K., Ohshima, T., Tanaka, S., Nagai, T., 1995. Biomechanical effects of shock-waves on *Escherichia coli* and lambda-phage DNA. Shock Waves 4 (6), 293–297.

Vitko, J., 2005. Sensor systems for biological agent attacks: protecting buildings and military bases. Technical Report, The National Academies Press.

Willeke, K., Baron, P.A., 2001. Aerosol Measurement: Principles, Techniques, and Applications. Wiley-Interscience, New York.

Zhang, Z., Ferenczi, M.A., Thomas, C.R., 1992. A micromanipulation technique with a theoretical cell model for determining mechanical-properties of single mammalian-cells. Chemical Engineering Science 47 (6), 1347–1354.

Zinin, P.V., Allen, J.S., Levin, V.M., 2005. Mechanical resonances of bacteria cells. Physical Review E 72 (6), 061907.1–061907.10.